Post-injection pilot: executed results

Local readability, directional evidence and finite-window limitations

Study ID: P01-ID1 | Results log v1.2 | 26 September 2026

This is a results log, not another journal manuscript. It records one specified computational pilot, its independent-method checks and its limits. The primary model family and outcome were recorded before execution. The sign tests, precision calculation and additional window/eligibility diagnostics below were added after the outcome was known; they are explicitly secondary reanalyses, not changes to the original study. No external preregistration, human specialist review, participant experiment or cosmological observation is claimed.

1. Main result

The source was switched off after injection. The predeclared change relative to matched frozen evolution was negative. A later factorial extension asks a different question by comparing two Hamiltonian orientations at fixed injection; its paired contrast is positive. Neither number replaces the other. At six qubits with rotated injection, the mean normalized change was **-0.015225**, with 68 negative and 28 positive unit-level contrasts. None of the 96 primary units produced a new singleton record satisfying the strict initial-information floor and error threshold throughout any declared half-unit window, in either frame.

The full source bit was not erased: the two global conditional states remained orthogonal under their shared unitary. Local access, transfer, redundancy and global information are different outcomes. There is no inference here that AIU or a general locality-record law is false.

2. Exactly what ran

There are **192 independent model/circuit units**, 96 at four qubits and 96 at six qubits. Each unit has two paired injection arms, giving **384 arm evaluations**, not 384 independent samples. Each arm is evaluated in two frames over 101 checkpoints. The primary statistic uses 50 positive-time checkpoints fixed before execution. The paired off-evolution control is analytic identity evolution, not a separately random sample.

The internal model is a random anisotropic nearest-neighbour Pauli chain with independent fields. It differs from an earlier review proposal that varied the amplitude of one fixed Hamiltonian shape. The alternate frame is an independent depth-two adjacent-pair Haar circuit. The graph and allowable readout algebras are supplied. Randomized coefficients do not make this a representative sample of all physical systems.

The executable simulation uses full finite-dimensional state vectors, not a quantum device. Runtime of the main numerical solve in this environment was approximately 2.08 seconds; that excludes writing, derivation, source checking and verification and is not a portable performance guarantee.

3. Primary and sensitivity results

Table 1. Baseline-subtracted local-readability contrast

Qubits	Injection arm	Mean z	Approximate bootstrap 95% interval	Positive / negative / tie
4	native	0.015125	[0.008577, 0.022237]	61 / 35 / 0
4	rotated	-0.028761	[-0.035284, -0.022440]	18 / 78 / 0
6	native	0.011674	[0.007238, 0.016167]	65 / 31 / 0
6	rotated	-0.015225	[-0.021070, -0.009646]	28 / 68 / 0

Only the six-qubit rotated arm is primary. The native-injection arm compares its native frame against the paired alternate frame, which is not its own physical injection frame. Do not pool the four rows as independent confirmations.

For the primary row, the distribution-free Hoeffding 95% interval is **[-0.292446, 0.261996]**. It crosses zero. The much narrower bootstrap interval is approximate and informative about this finite empirical distribution; it is not a distribution-free guarantee or a confirmation of a universal negative sign. This original sample does not support a positive value of its own target. It cannot isolate the effect of changing the dynamics-locality frame, which it held fixed.

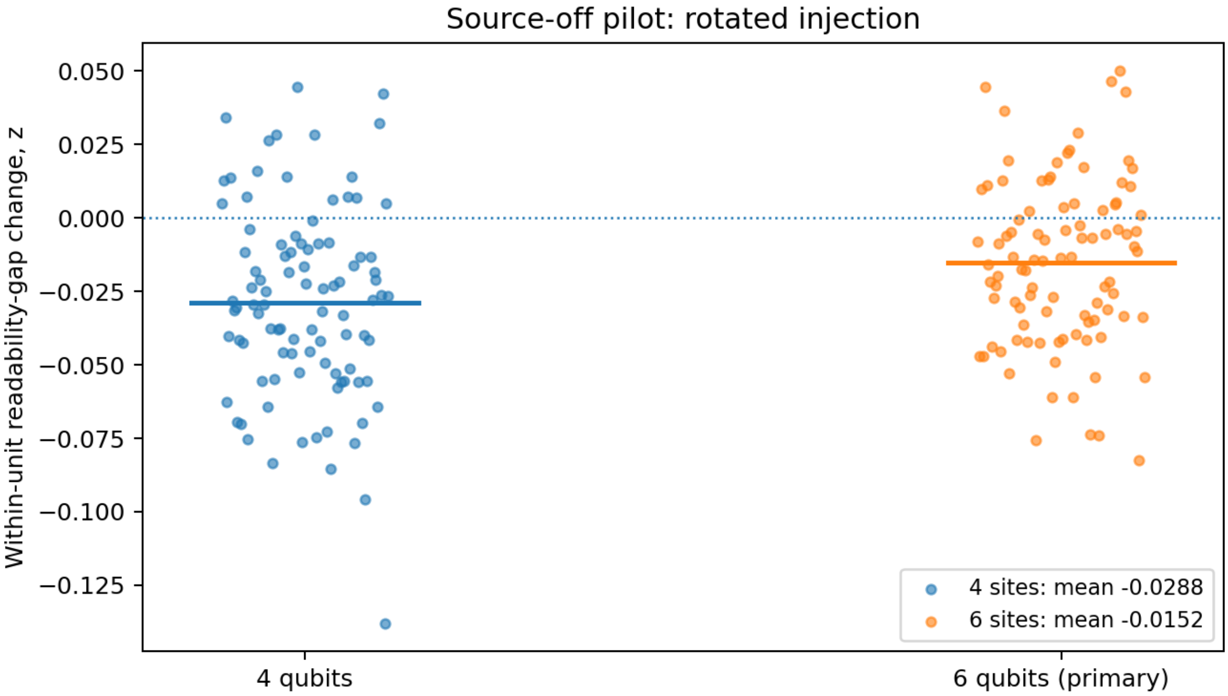

Figure 1. Each point is one independent model unit. Zero is no change in the readability gap relative to the no-evolution baseline. This is not a probability of AIU or a test of the older LRA-count margin.

3.1 A negative change does not mean C has better absolute readout

For the six-qubit rotated arm, mean singleton trace distance at switch-off was approximately **0.208408 in L** and **0.166667 in C**. The corresponding post-time averages were **0.197702 in L** and **0.186411 in C**. Thus L's initial gap of **0.041742** narrowed to **0.011292**. Half that gap change is the negative primary result. Claiming that records migrated to C would overstate this statistic.

A scrambled representation can spread partial distinguishing information over multiple sites; sums of singleton distances are not additive global information. The primary mean therefore measures accessibility, not independent bits, redundant strong records or a unique preferred subsystem structure.

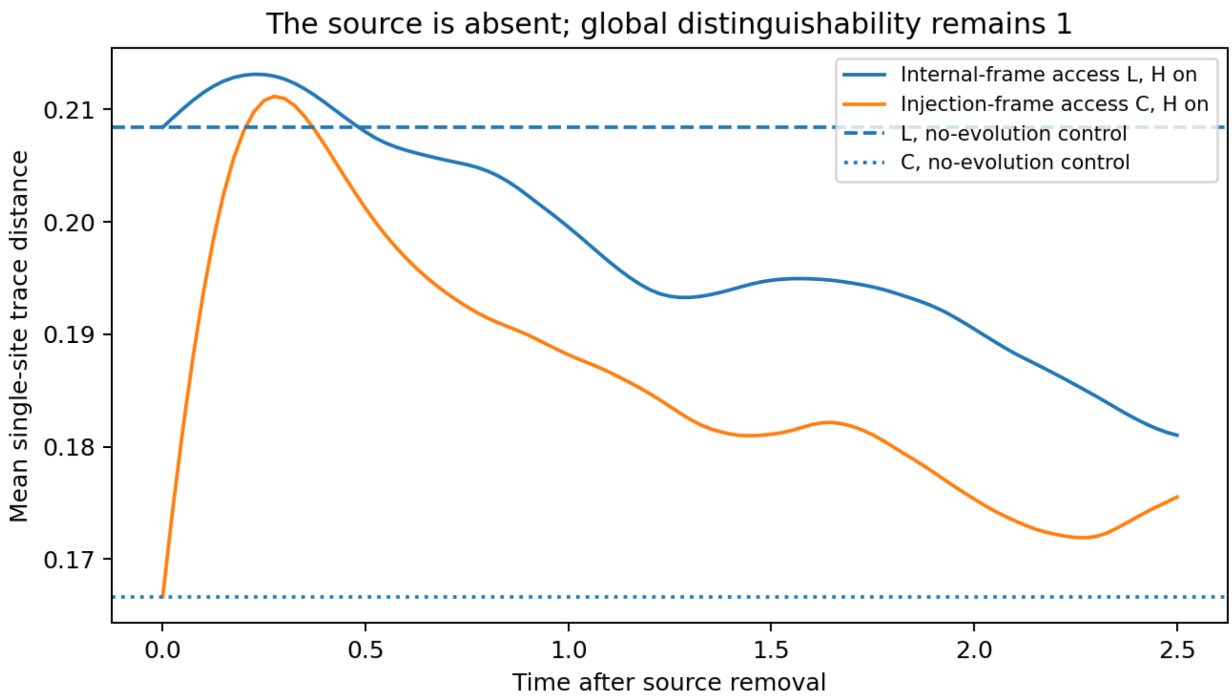

Figure 2. Six-qubit rotated injection, means across 96 units. The pulse ends at t=0; the source is absent thereafter. Horizontal baselines are the matched frozen states. Weak local readability can change even when no new fragment meets the strict record criterion.

3.2 Post hoc directional analysis

Let p_{pos} be the probability of a positive nonzero unit contrast. The exact sign test evaluates $H_0 : p_{\text{pos}} = 1/2$ with independent signs. It does not assume symmetry of the full contrast distribution, but independence alone is not the null. It is not a test of zero mean. Ties use the original 10^{-12} reporting tolerance; none occur, and the smallest absolute contrast across these data is greater than 2.5×10^{-4}.

Table 2. Post hoc two-sided binomial sign tests

Qubits / arm	Positive / negative	Unadjusted p	Holm-adjusted p, four-row family
4 / native	61 / 35	0.0103459	0.0103459
4 / rotated	18 / 78	4.44694e-10	1.77877e-9
6 / native	65 / 31	0.000674719	0.00134944
6 / rotated	28 / 68	0.0000545915	0.000163775

The adjustment covers these four tests and does not require independence between the paired arms. It does not account for unrestricted post hoc exploration outside this stated family. Within the explicit sampling law, the rotated-arm signs provide strong secondary evidence against directional balance. This neither makes the mean a distribution-free finding nor overturns the formal distinction between the executed readability target and the older LRA hypotheses. The predeclared bootstrap interval already provided approximate evidence about the mean; it was not an empty or wholly inconclusive result.

3.3 Precision limitation, not a retrospective power claim

At 96 units, the chosen range-only Hoeffding half-width is 0.277221. Solving $\sqrt{2\log(40)/N} \leq 0.015$ gives $N \geq 32791$. This is a sufficient worst-case sample count for that confidence-interval precision, not a minimum sample size required by every valid method and not a power calculation. The width is much larger than the observed effect. The pre-execution plan should have stated this limitation, and the original plan is preserved without retrospective amendment. Future studies should distinguish a justified precision budget, an alternative-specific power analysis and computational feasibility. This calculation is not a recommendation to run 32,791 units.

4. Strict new-record criterion

The criterion required initial error at least 0.4999 and subsequent error at most 0.1 throughout [0.5,1.0], [1.0,1.5], [1.5,2.0] or [2.0,2.5]. At both sizes and in both arms, every possible upper count for a new singleton record was zero in every window. Here that was not an unequal-certificate problem: the initial-information floor or a failing checkpoint already ruled out the strict condition numerically. The raw data retain all cases.

This says nothing about larger fragments, looser tolerances, other windows, different preparation laws or other Hamiltonians. Those would be different analyses. They were not added after observing this outcome. The numerical guard remains empirical rather than a formally certified roundoff enclosure.

4.1 What the zero count excludes, and what it does not

A review-stage diagnostic of the original stored trajectories separates transient access from full-window persistence. In the native arm, 5 initially eligible site/unit pairs at four qubits and 10 at six qubits briefly reached trace distance at least 0.8 at a positive-time checkpoint. None satisfied a complete declared window. These are site/unit pairs, not independent samples or counts of distinct systems; they are not new strong persistent records. Thus the data themselves do not support the general statement that internal dynamics cannot create local source accessibility. In the rotated arm, none of the initially eligible singletons reached this strict checkpoint threshold within the recorded horizon.

Initial eligibility also differs between frames because partial source information can already be distributed at switch-off. At six qubits with rotated injection, 288 of 576 site/unit pairs are initially eligible in L, compared with 480 in C. The definition deliberately asks about newly informative fragments, so this difference is part of the target, not a reason to remove inconvenient units. The companion mean-readability statistic has a different denominator and remains unchanged. The full diagnostic table is supplied in the supplement and data.

5. Transport worked in the analytical controls

For the vacuum-versus-excitation encoding, the two-site exchange control gives recipient distinguishability $\sin^2 t$. At $t = \pi/2$, the source bit has transferred from the addressed site to its neighbour. Four- and six-site exchange chains matched an independently evaluated one-excitation hopping model. The sampled end-site distinguishability reached approximately 0.972655 at time 2.80 for four sites and 0.911536 at time 3.95 for six sites. These are sampled control values, not globally optimized arrival times or claims of new transport physics.

For a vacuum-versus-single-excitation code, let $p_j(t)$ be the excitation probability. Then $d_j(t) = p_j(t)$ and $\sum_j p_j(t) = 1$. Error at most 0.1 requires $p_j \geq 0.8$, so at most one singleton can qualify at one time. This control demonstrates transport without high redundant copying. It exposes why a redundancy measure is not automatically a transport or geometry-recovery measure.

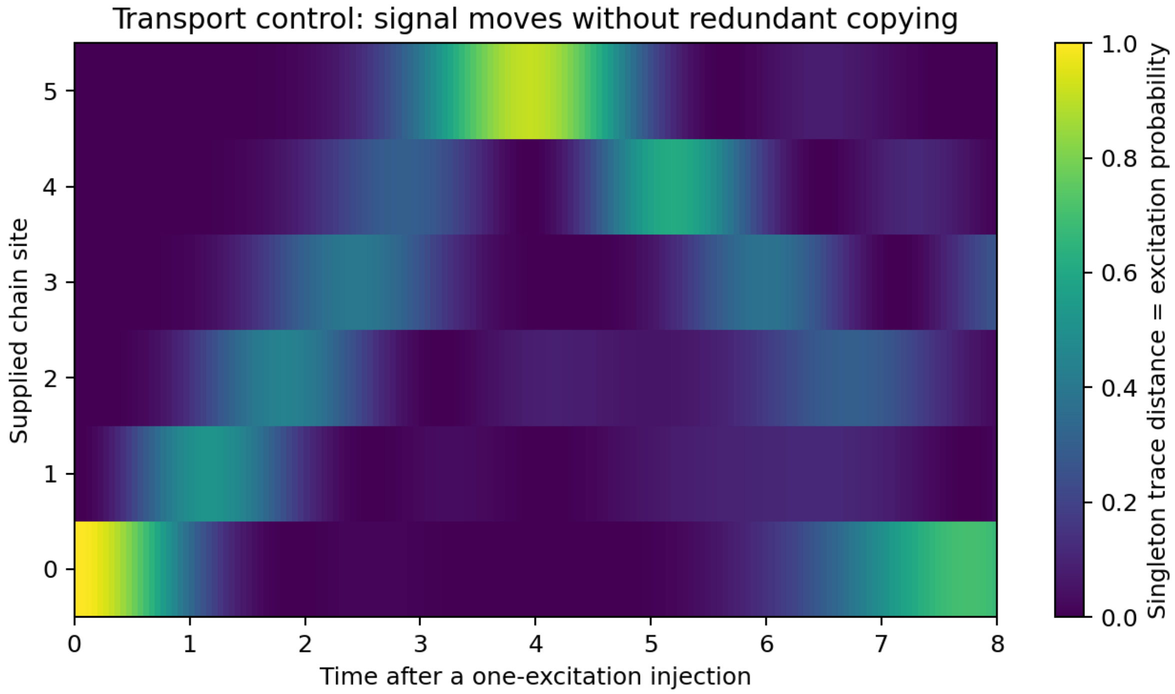

Figure 3. Full-state calculation, independently matched to the one-excitation reduction. Propagation is present although conservation limits simultaneous strong singleton records. The chain and its coordinates are supplied.

5.1 Transport-window and source-encoding diagnostic

The original windows end at 2.5. In the uniform exchange-chain control using a vacuum-versus-excitation code, end-site distinguishability is $|f(t)|^2$. On the reviewer's 0.05 grid, it exceeds 0.8 during 2.4 to 3.2 at four sites and 3.6 to 4.3 at six sites. No complete declared half-unit window lies inside either interval. This is a valid warning that the windows cannot assess late far-end strong transfer in that control.

The actual pilot uses opposite-phase superpositions of vacuum and a single addressed excitation, not that control's source code. For the ideal number-conserving exchange chain with the pilot code, direct partial trace instead gives end-site distinguishability $|f(t)|$. Its qualification threshold corresponds to excitation probability 0.64, not 0.8. Both curves and their exact declared-window checks are supplied. No complete original window passes at the far end for either encoding, but the two threshold times must not be interchanged.

These controls do not establish that all zero counts in random anisotropic chains were built in: those chains, their code, distances and eligible fragments differ, and some near-site transient strong signals were observed. The defensible conclusion is narrower: the strict result is conditional on a restrictive floor, threshold and short windows and cannot stand for absence of transport. No late-window rerun or changed primary endpoint is included in this release.

6. Verification

A separate implementation does not import the main solver. It propagates selected n=4 and n=6 units using exponential action and reduces full density matrices rather than the main state-tensor shortcut. The largest compared trace-distance discrepancy was **9.104e-15**. The largest main-run norm error was **3.320e-14** and the largest branch overlap magnitude **2.371e-14**.

The **36 checks passed**, with **0 failures**. These checks include selected-trajectory agreement, zero evolution, identical branches, passive conjugation, two-site transfer, one-excitation conservation, closed stationary records and amplitude-damping erasure. They are not 36 independent physical experiments. Numerical agreement is not a formal floating-point proof.

A closed diagonal Hamiltonian preserves orthogonal product records because their density matrices commute with H. Conversely, an ordinary amplitude-damping channel reduces the distinguishability of zero-versus-one states as e^{-t}. These elementary controls correct the overstatement that persistence always requires a large or dissipative environment. What matters is the stated retention mechanism and observable, not openness alone.

7. Decision after the pilot

Keep the original result and the new counterfactual separate. The source-off pilot measures a change from frozen evolution with the dynamics always native to L. Its negative mean is reproducible but is not an isolated causal estimate of locality. The factorial extension varies that dynamics frame at fixed injection and produces a positive paired intervention contrast. It adds missing information rather than changing the original question after the answer was seen.

This is not recovered locality: the frames, Hamiltonian family and readout rules are all supplied. A named Lieb-Robinson mechanism has not been identified merely by obtaining a positive scalar contrast. An actual identification study would require multiple injections, a reconstruction method not given its target and held-out prediction. An open-system retention study separately needs a justified reservoir and erasure controls. Neither extension is silently announced as completed here.

8. Reproduction and provenance

pilot/PRE_EXECUTION_PLAN.md, pilot/config.json and pilot/PRE_EXECUTION_RECEIPT.json retain the pre-outcome specification and local hashes. data/pilot_run/model_inputs.json contains coefficients and random-stream identifiers. trajectories_n4.npz and trajectories_n6.npz contain raw per-site readability and small validation examples. per_unit.json retains the count bounds and all individual outcomes. code/run_injection_pilot.py refuses a nonempty output directory. The reviewer bundle includes the text, configuration and code but omits binary trajectories to remain small.

No email was sent and no external review occurred. The specialist brief accompanies *Frame-Aligned Records* and its supplement for a later, separately authorized circulation.

9. Review-stage reimplementation and factorial intervention

9.1 Same target, fresh reimplementation

An independently written implementation supplied during review uses the protocol's model law, 50 positive-time readouts, a two-layer adjacent-pair Haar circuit and fresh seeds. Its author had to infer the open-chain convention, the order $U_C = L_2 L_1$, and the leftmost addressed site. Those inferred conventions were compared with the original code, not certified by initial eligibility counts alone. Matching a small diagnostic does not logically prove complete implementation identity.

All supplied numerical summaries were re-executed with their stated seeds. The six-qubit 60,000-unit rotated run gives mean -0.01412453 and a range-only 95% interval [-0.02521338, -0.00303568]. This is a new sample from the explicit law, not a retrospective increase of the original 96-unit sample. Its prediction file was supplied with a matching hash; a local hash establishes integrity, not an externally certified time of creation.

9.2 The added factor and its estimand

For each paired unit, injection in L or C is crossed with dynamics $H_L = H$ or $H_C = U_C H U_C^{\dagger}$. Readout remains in the same L and C algebras. Let g_b^a be the post-time mean readability gap and g_0^a its common initial gap at injection a. Then

$$z_{ab} = \tfrac{1}{2}(g_b^a - g_0^a), \qquad e_a = z_{aL} - z_{aC} = \tfrac{1}{2}(g_L^a - g_C^a).$$

The baseline cancels in e_a, so $-1 \leq e_a \leq 1$. The factorial contrast is not the old z_{CL}, and a positive e_C need not make either z_{CL} or z_{CC} positive. At six qubits the four means are:

Injection	Dynamics L	Dynamics C	Difference
L	0.01400416	0.00349055	0.01051361
C	-0.01402828	-0.02666340	0.01263512

The values were reproduced, not merely transcribed. The factorial code originally retained aggregate JSON only. This replay additionally retains per-unit z and before/after readability in NPZ arrays, with the original seeds and input-generation code unchanged. It does not retain every factorial state trajectory.

9.3 Finite-family sampling uncertainty

The six disclosed contrasts cover two injection conditions at each of four, six and eight qubits. The four- and six-qubit runs contain 20,000 independent model units per size; the eight-qubit run contains 1,000. Four arms within one unit are paired, not four independent observations. A simultaneous empirical-Bernstein bound uses the paired sample variance, rescaling from [-1,1] and allocating error over both tails and six targets [Maurer and Pontil 2009, Theorem 4].

Qubits	Injection	Mean e	Simultaneous 95% Bernstein interval
4	L	0.005752	[0.003528, 0.007976]
4	C	0.011074	[0.008801, 0.013347]
6	L	0.010514	[0.008604, 0.012423]
6	C	0.012635	[0.010692, 0.014579]
8	L	0.010363	[-0.020023, 0.040748]
8	C	0.012137	[-0.018361, 0.042634]

This finite-sample result assumes iid units under the declared law and faithful numerical evaluation. It makes no normal-distribution assumption, but it does not account for unlimited undisclosed model selection. The variance-sensitive analysis was specified during this review, after the supplied summaries were known. It is a disclosed secondary analysis, not a newly preregistered confirmatory study. The older normal-approximation intervals and wider simultaneous Hoeffding intervals are all retained in the CSV, not selected according to which exclude zero.

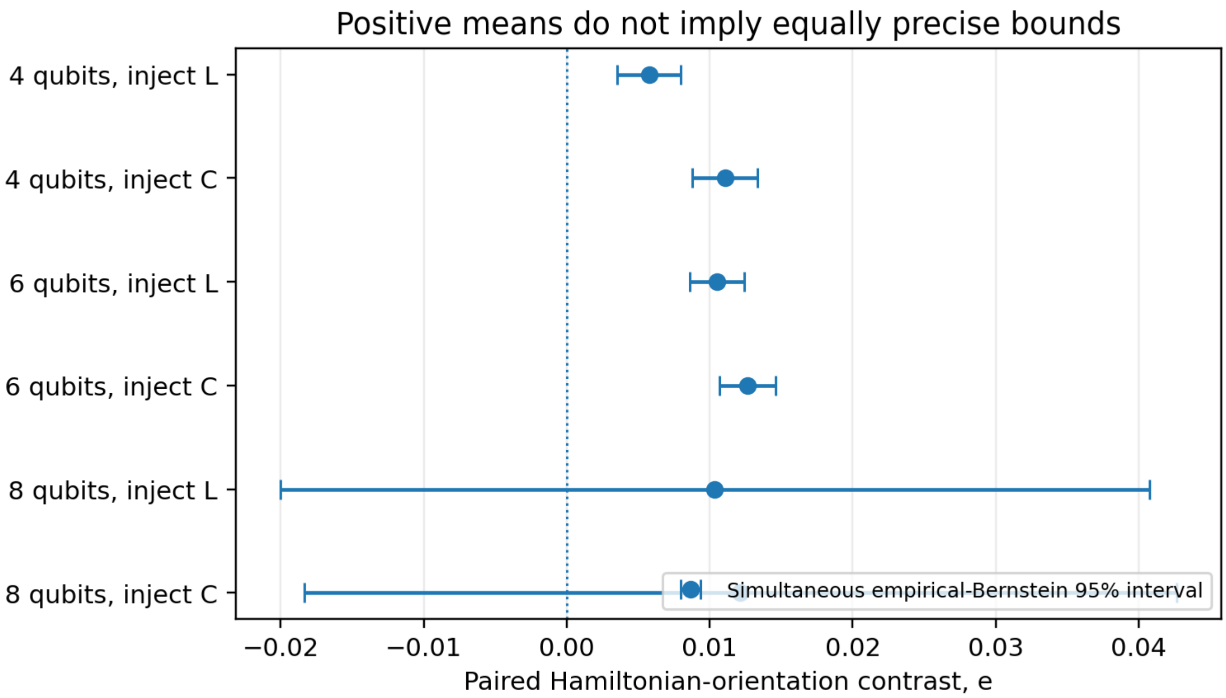

Figure 4. Different uncertainty methods answer the same six factorial targets. Normal intervals are approximations; the displayed Bernstein intervals use the stated finite-sample assumptions and six-target coverage. These are not confidence intervals for AIU or emergent spacetime.

9.4 What the extension identifies

The intervention changes the whole Hamiltonian's orientation relative to fixed preparation and access. Its spectrum is unchanged, but the prepared energy distribution and detailed state-dynamics relations need not be. Thus the contrast supports a specified model intervention, not a pure effect of locality with all other relevant properties held constant. A third independent circuit frame W has intermediate supplied mean outcomes; there is no theorem that it must be neutral or intermediate.

The small nonzero interaction between injection and dynamics also means that a unique additive attribution to an injection mechanism and a locality mechanism is not supplied. A regression of z on its initial gap contains an algebraic minus-one-half term by definition. Such regression is descriptive unless additional assumptions identify the mechanism; an intercept at zero gap is not by itself proof of frame selection.

Lieb-Robinson bounds constrain propagation for appropriately local interactions. They do not imply the observed sign of the average-readability intervention. Both Hamiltonians are related by a fixed-depth local circuit, which enlarges native support only by a bounded amount. Distinguishing this explanation from other finite-family effects requires an independently chosen response or intervention test.

9.5 Reproduction boundary

The original pre-execution plan, configuration, code and receipt remain immutable. Supplied review predictions, including the failed near-zero factorial prediction, are preserved. Re-execution is not external scientific replication and does not verify the claimed chronological creation of those review predictions. Selected factorial trajectories were checked with exponential action and full-density-matrix partial traces rather than the source's spectral/Bloch implementation; the separate check report records its actual scope.

New commands and numerical assumptions are in the Supplementary Information. The archive includes the original source-off trajectories, new factorial unit summaries, all three supplied review scripts, reference outputs and fresh replay outputs. No outside correspondence, peer review or publication was performed.

10. Secondary-analysis sources

The exact binomial calculation follows directly from independent equiprobable signs under the null. See Penn State STAT 415, Section 20.1, *The Sign Test for a Median*, for the median interpretation and its distinction from a mean test. The original contrast data, rather than only the rounded summary, are used by code/analyze_review_additions.py. It also reconstructs each unit contrast from raw trajectories and writes the four-row sign tests, transport-encoding curves and initial-eligibility diagnostics. These are analyses of the same pilot, not independent replication.

The mathematical source of the range-only confidence bound remains Hoeffding (1963), cited in the methods paper. Holm adjustment is applied to the four disclosed post hoc sign tests; it does not make them predeclared. No new participant, cosmological or quantum-device data were collected.

Holm, S. (1979). A simple sequentially rejective multiple test procedure. Scandinavian Journal of Statistics 6(2), 65-70. https://www.jstor.org/stable/4615733

Penn State STAT 415. Section 20.1, The Sign Test for a Median. https://online.stat.psu.edu/stat415/lesson/20/20.1

Maurer, A., and Pontil, M. (2009). Empirical Bernstein Bounds and Sample Variance Penalization. COLT 2009. https://arxiv.org/abs/0907.3740